

Supplementary Information

Nanocarrier Foliar Uptake Pathways Affect Delivery of Active Agents and Plant Physiological Response.

Hagay Kohay¹, Jonas Wielinski¹, Jana Reiser¹, Perkins Lydia A²., Kurt Ristroph³, Juan Pablo Giraldo⁴, Gregory V. Lowry¹.

¹ Carnegie Mellon University, Civil & Environmental Engineering, Pittsburgh, PA.

² Molecular Biosensor & Imaging Center (MBIC), Carnegie Mellon University, Pittsburgh, PA.

³ Purdue University, Agricultural & Biological Engineering, West Lafayette, IN.

⁴ University of California, Botany & Plant Sciences, Riverside, Riverside, CA.

*Corresponding author: Gregory V. Lowry (glowry@andrew.cmu.edu)

Table S1. Size parameters obtained by DLS, TEM, and zeta potential measurements for L-LDH and S-LDH.

	Intensity average size (nm)	Number average size (nm)	PDI	Size by TEM (nm)	ZP (mV)
L-LDH	121±6.5	53±9	0.19	57±20	+36.6±0.2
S-LDH	69.43±1.3	37±1.5	0.13	43±13	+38.6±1.0

TEM measures the primary particle size directly, but the average size is based on a relatively small population of particles. In contrast, DLS measures the hydrodynamic diameter of the particles. This is based on an indirect measurement of the fluctuation of the light scattering from the sample, but the results are based on a much larger population of particles. The trends in both measurement methodologies (DLS and TEM) were similar, with smaller and more homogenous particles formed when using the MIV mixer.

Table S2- Crystallite size of LDH in 110 and 003 planes.

	d(ang.)	2θ(deg)	FWHM (deg)	Crystallite size (nm)
S-LDH-003	0.779	11.32	0.94	8.5
S-LDH-110	0.153	60.42	0.49	32.5
L-LDH-003	0.795	11.12	0.743	10.8
L-LDH-110	0.154	60.2	0.57	27.8

Both LDH particles show similar d-spacing: 0.78 nm for S-LDH and 0.795 nm for L-LDH related to mostly Cl⁻ as an exchangeable anion in the LDH structure [1]. The distance between two adjacent metals in the plates was $a=2*d(110)=0.307\pm 0.01\text{nm}$ for both LDH [1]. The Z-axis crystallite size of the LDH particles was 8.5 nm and 10.8 nm as calculated using the Scherrer equation indicating ~11 and ~14 layers of LDH for S-LDH and L-LDH respectively.

Table S3. Descriptive statistical analysis for the TEM images. The size difference was found statistically significant using two samples t-test ($P < 0.000033$)

Data	N total	Mean (nm)	Standard Deviation	Minimum	Median	Maximum
S-LDH	55	43.4	13.1	19.8	41.9	74.6
L-LDH	70	56.6	19.5	20.3	55	107

Table S4. Release of Tb from L-LDH, tested after dilution of 1:2 with DDW and APS and compared to the Tb salt, solutions were equilibrated for 1 day.

	Tb released (%)
L-LDH-13 ppm water	0.0024±0.0003
L-LDH-13 ppm APS	0.056±0.009
Tb 13 ppm	95.04

Table S5. Complete quantification of Tb attachment to the leaves upon washing and Tb in the washing solution following adaxial and abaxial application of Tb salt and L-LDH doped with Tb.

	Av. Tb washed off the leaf (%)	Av. Tb associated with the leaf (%)	Total (%)	Relative association of Tb
Tb salt adaxial	52.2 ± 11.4	28 ± 6.3	80.2 ± 13	0.35
L-LDH adaxial	8.6 ± 1.4	84.5 ± 17.3	93.1 ± 17.4	0.91
Tb salt abaxial	45.1 ± 16.3	35.6 ± 10.9	80.7 ± 19.6	0.44
L-LDH abaxial	5.5 ± 1	76.2 ± 12.8	81.7 ± 12.8	0.93

Table S6. Parameters related to the adsorption and desorption of ssDNA-Cy3 from L-LDH surface, L-LDH at 0.7 g/L, and ssDNA-Cy3 at 0.04 g/L.

	Cy3 adsorbed (%)	Cy3 negative sites (mmol/g)	AEC LDH (mmol/g)	LDH compensated sites (%)	Cy3 release upon washing with DDW (%)
L-LDH	90.3±6.1	0.098	3.3	~3	0.15± 0.08

The adsorption of ssDNA (0.04g/L) by the surface was 90% and the release from the surface, tested with Double distilled water solutions was negligible. Calculating the amount of LDH positive sites compensated by the ssDNA oligomer was found to be 3% of the overall positive sites on the surface. Accordingly, it is reasonable to expect that only the external surfaces of LDH are available for adsorption in these conditions [2].

Tables S7. Size and ZP of S-LDH and L-LDH upon adsorption of ssDNA-Cy3 at different concentrations and in 10 mM MES buffer solution, ZP was measured in water.

Batch	Z-Average	Number size (nm)	PDI	ZP (mV)	Used for confocal
S-LDH	60±0.8	37±1.5	0.13	49.2±0.4	
S-LDH-Cy3 0.04 g/L	124.4±3.5	55.6±22	0.19	52±3	V
S-LDH-Cy3 0.06 g/L	132±4	80±9	0.15	50±0.3	
S-LDH-Cy3 0.08 g/L	195±7	129±20.6	0.16	46.1±1.1	
S-LDH in 10 mM MES buffer solution	60±0.7	38±1	0.252		
L-LDH-Cy3 0.04 g/L	154±2.4	76±8	0.24	55±4	

Table S8. A summary of parameters describing the properties of the leaves and S-LDH coverage in different sections.

	Adaxial	Abaxial
Stomata density (#/mm ²)	2.8±6	157±27
Potential stomata coverage (%)	0.011±0.02	0.74±0.22
LDH coverage on cuticle (%)	11.23±1.75	10.06±1.29
Stomata area covered by LDH (%)	*	57.7±20
Clogged stomata (%)	*	63±22

*Few to measure

Table S9. The mass ratio between sections of plants' organs after abaxial and adaxial applications and control plant based on Figure 4a.

	Treatment/Control mass ratio			
	Roots	Unexposed leaves	Main shoot	Total
Abaxial	1.12±0.14	1.51±0.49	1.18±0.23	1.21±0.13
Adaxial	1.17±0.14	1.33±0.47	1.31±0.23	1.29±0.17



Figure S1. Foliar application of LDH solution on the adaxial side (left) and abaxial side (right) of tomato.

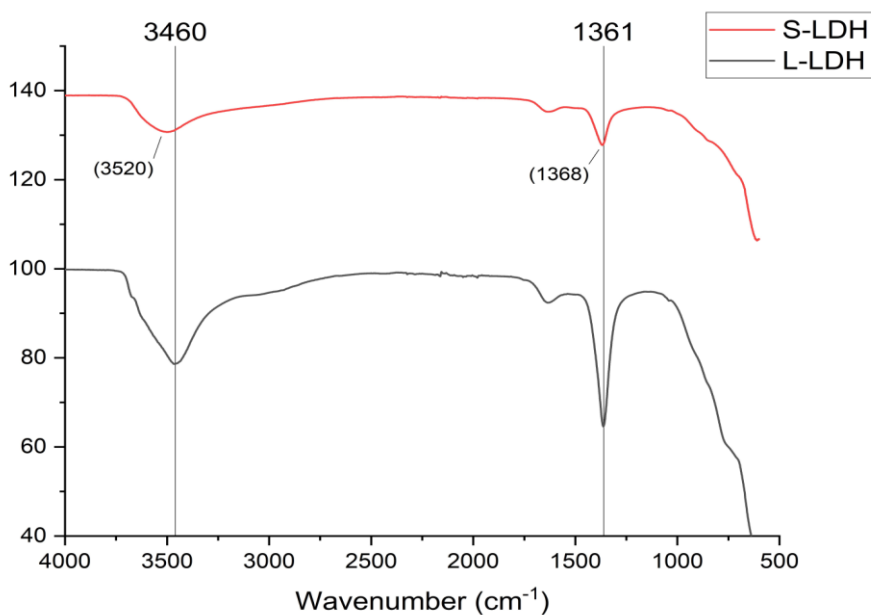


Figure S2. S-LDH and L-LDH characterization, ATR spectra.

Although both synthesis pathways produced LDH some chemical differences can be observed by the ATR spectra. The main difference is a blue shift for S-LDH in comparison to L-LDH. L-LDH display peaks at 1361 and 3458 cm^{-1} assigned to carbonate and OH stretching vibrations of the OH groups, respectively. For S-LDH these two peaks blue shifted to higher wavenumbers 1368 and 3520 cm^{-1} , respectively. The shift at 1361 to 1368 cm^{-1} can be attributed to a differentiation in the exchangeable anion [1,3].

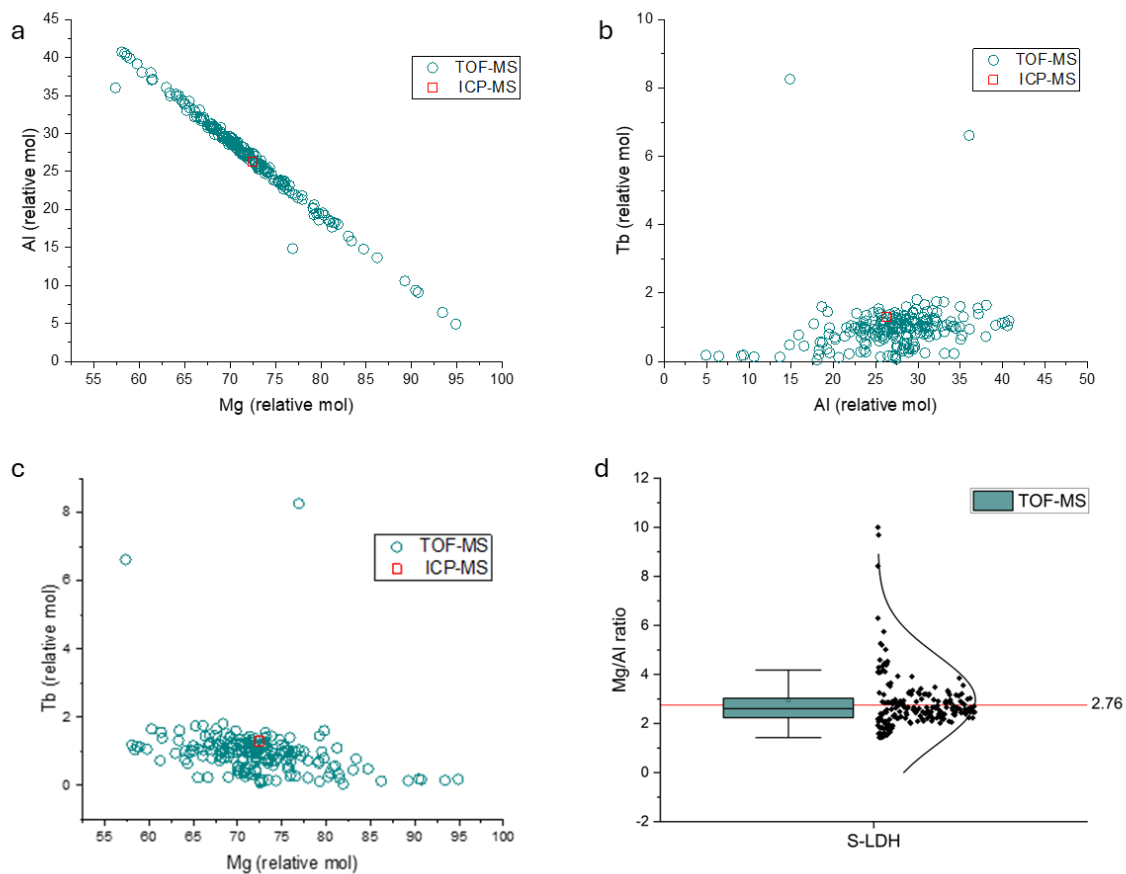


Figure S3. Characterization of Tb-doped S-LDH. (a-c) The molar ratio of the metals integrated in S-LDH NP as was measured by single particle ICP-TOF-MS. (d) Distribution of Mg/Al ratio of S-LDH population obtained by single particle ICP-TOF-MS, the red square/line represents the values obtained by ICP-MS.

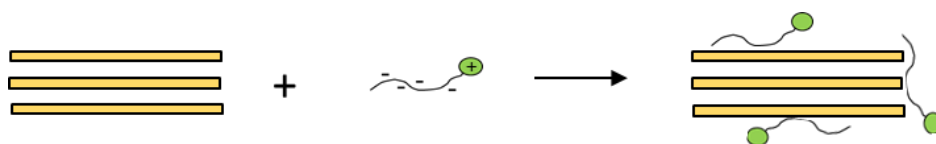
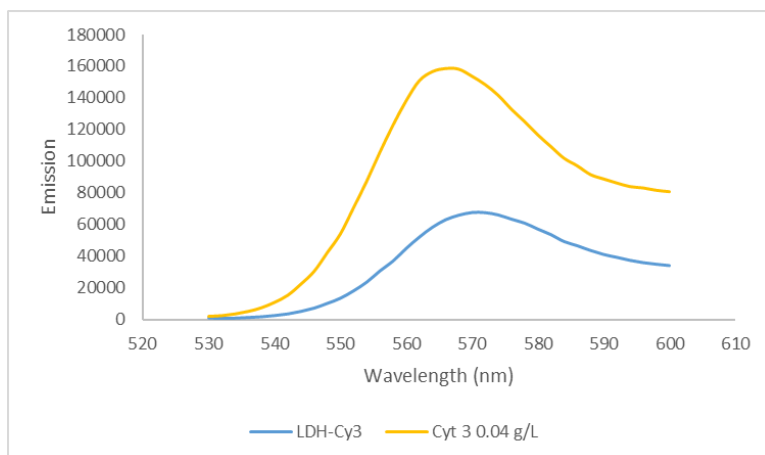


Figure S4. An illustration of the adsorption process of ssDNA-Cy3 to the S-LDH surfaces, multiple electrostatic interactions are suggested as the main adsorption mechanism, the positive charge on the Cy3 end enables to sustain of the positive charge on the surface.



Fluorescence of LDH-Cy3 complex	Cy3 related concentration (g/L)	Expected concentration (g/L)
19793±1282	0.01±6.4E-4	0.032±0.002

Figure S5. (a) Quenching and shifting upon adsorption of ssDNA-Cy3 to L-LDH. (b) ssDNA-Cy3 fluorescence upon adsorption to L-LDH, fluorescence quenched substantially upon adsorption.

Further validation for the interaction between LDH and ssDNA-Cy3 was obtained by characterizing the fluorescence of Cy3 in its attached form. Upon adsorption a quenching and a red shift (4 nm) can be seen; the emission value of the attached Cy3 was 3 times lower than the expected value based on the adsorbed amount.

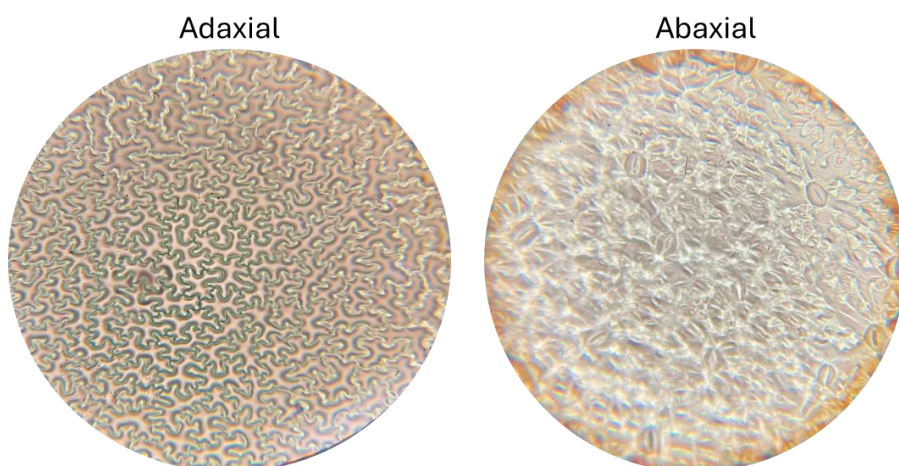


Figure S6. Image of tomato cuticle from adaxial and abaxial side upon peeling using light microscopy, 40X magnification.

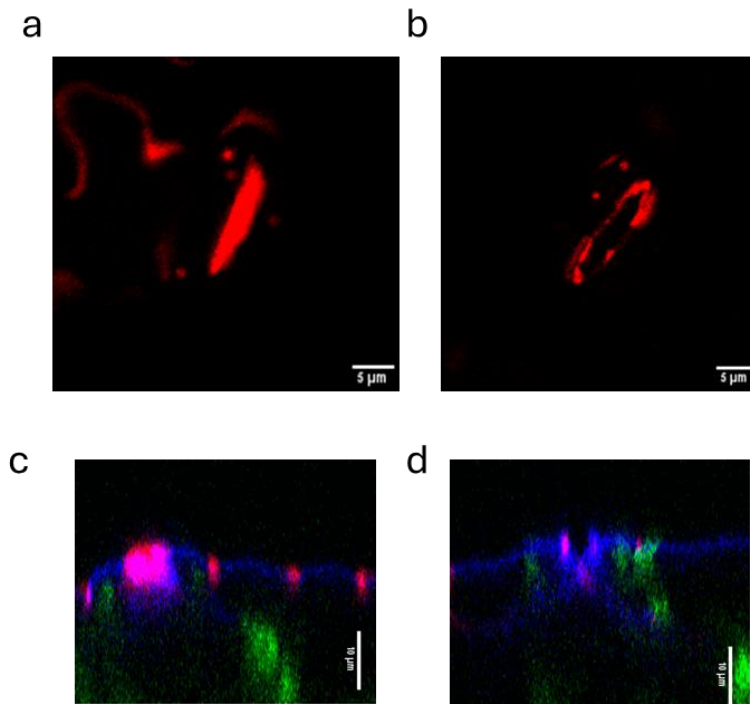


Figure S7. (a) Images of S-LDH colocalized in the stomata and (b) open stomata (right). (c) z-profiles of S-LDH colocalized in the stomata and (d) open stomata. Blue-cuticle, red-S-LDH, green-chlorophyll fluorescence.

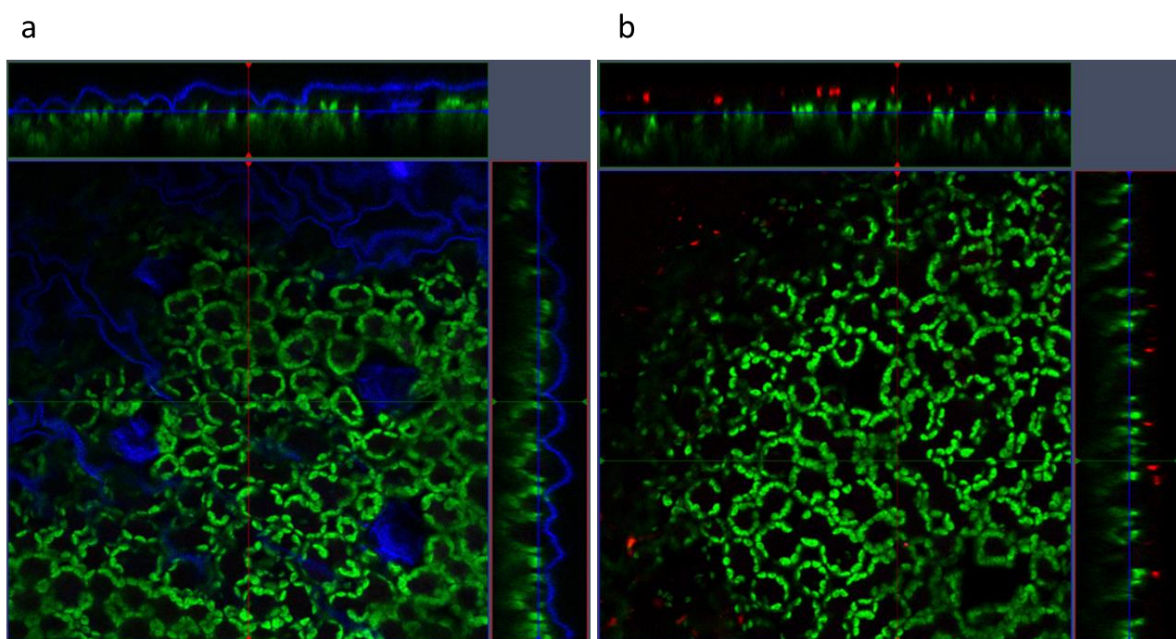


Figure S8. Fluorescence emitted from the leaf under the experiment conditions showed no overlapping in the components' spectra. In both cases, all 3 fluorescence channels were applied, and the same parameters were used to display the results. (a) Auramine O- 1 g/L. (b) L-LDH.

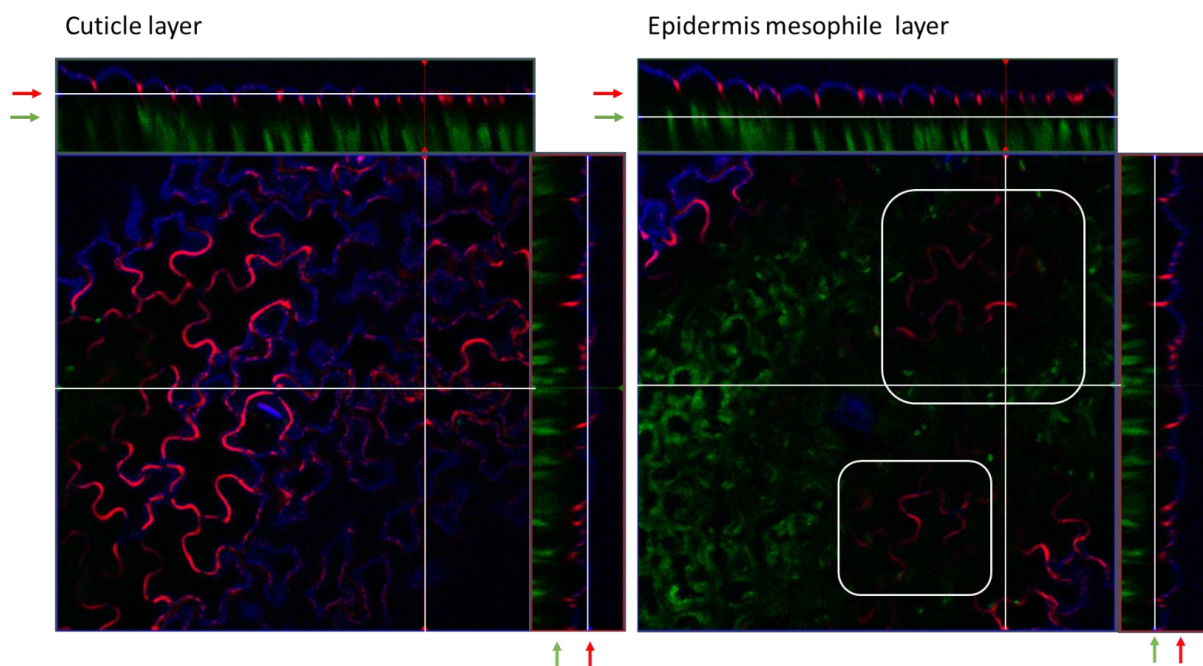


Figure S9. S-LDH NP penetrate through the cuticle to the depth of the epidermis layer. S-LDH application from the adaxial side of tomato leaf imaged after 20 h. The right image is related to the cuticle layer; the left image is related to the epidermis-mesophyle layer. Red, blue, and green represent NP, cuticle dye, and chloroplast, respectively. For each image the side and upper box represent the z-profile and the main image represents the surface of the leaf. The z-profiles describe the section marked by the white line on the surface (parallel to the line). In the profiles, white lines indicate the depth at which the fluorescence in the main images is being monitored. Squares represent the area where the NPs can be seen but no cuticle dye can be monitored.

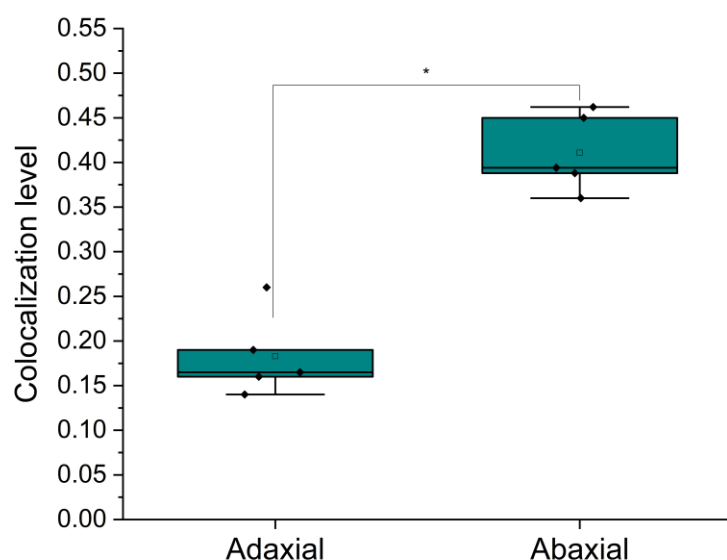


Table S10. Intensity colocalization levels of S-LDH in the cuticle in the z-profiles of the leaves obtained by Mander's coefficient, done of segments without stomata, n=5. Statistical analysis was done using one-way ANOVA followed by Tukey test, significance level for * $p < 0.05$.

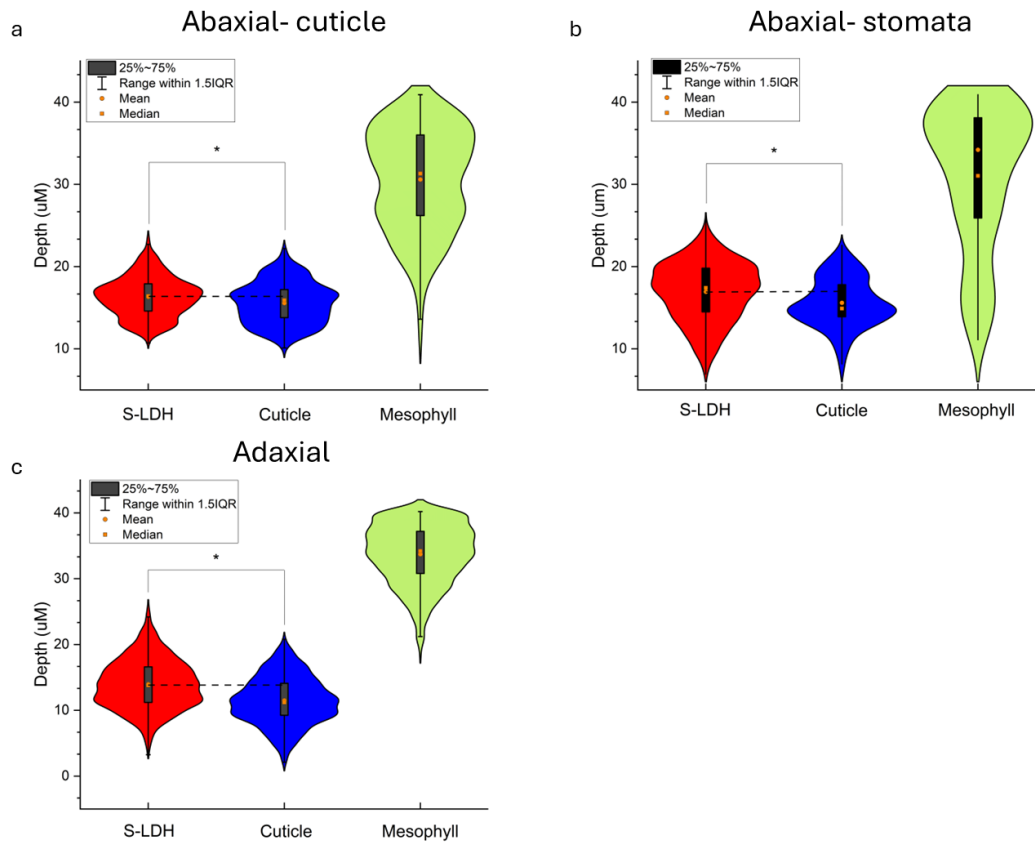


Figure S11. (a-c) Displays of the z-position of S-LDH compared to the cuticle and the mesophyll, were calculated by the 3D representation of z-stacks images (Imaris). (a) Abaxial application-cuticle segment. (b) Abaxial application-stomata segment (c) Adaxial application.

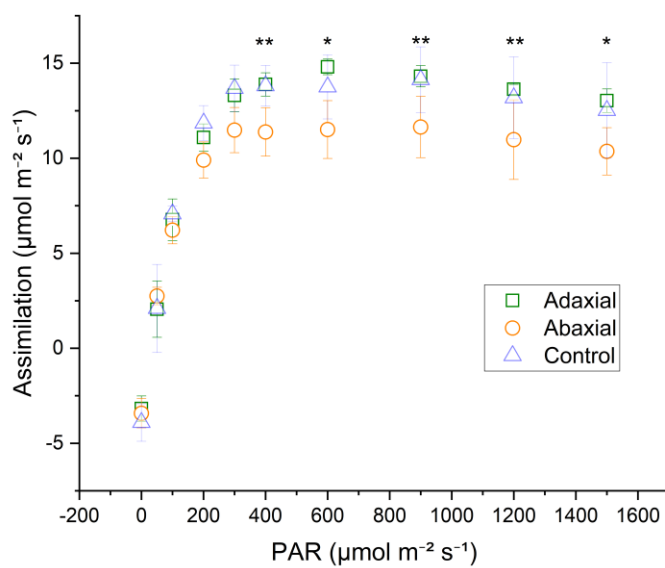


Figure S12. CO_2 assimilation rate as a function of light intensity (PAR) and S-LDH application. Statistical analysis was done using t-test, with a comparison between adaxial and abaxial. Significance level for * $p < 0.01$, ** $p < 0.05$, errors represent SD, $n=4/5$.

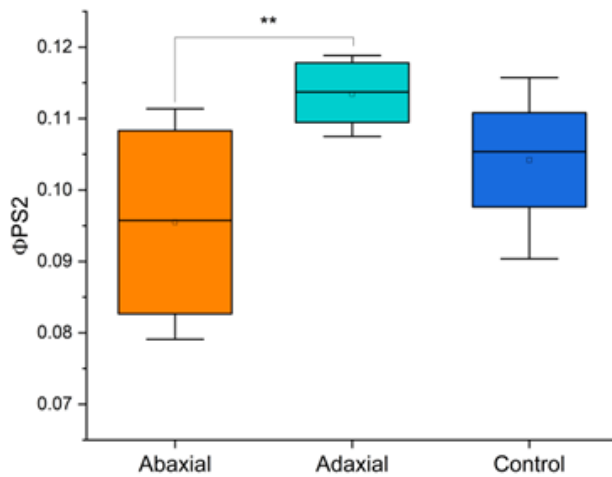


Figure S13. ϕ PS2 compared between adaxial and abaxial application of LDH at 0.15 g/L, light intensity of $1200 \mu\text{mol}\cdot\text{m}^{-2}\cdot\text{s}^{-1}$. Statistical analysis was done using a t-test, significance level for ** $p < 0.05$, $n=4/5$, errors represent SD.

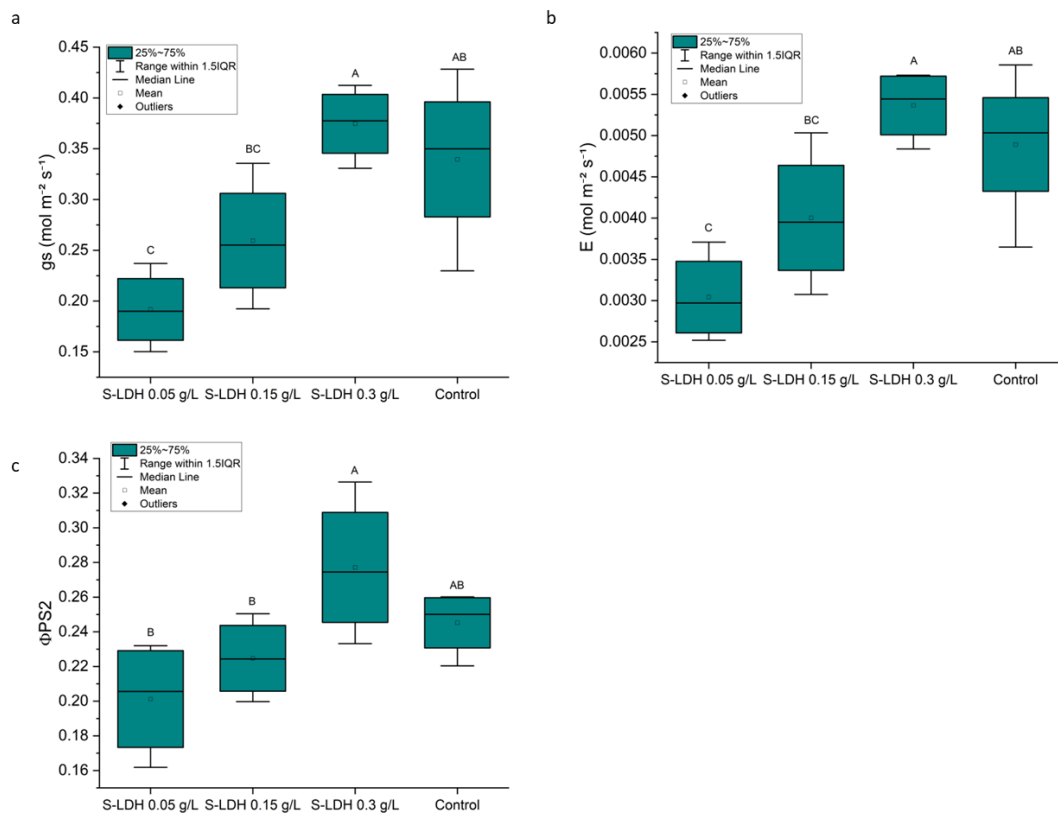


Figure S14. (a) g_s - Stomata conductance. (b) E -transpiration and (c) ϕ PS2 of tomato plant after abaxial applications as function of S-LDH concentrations, no deficiencies in the background solution (1/4 Hoagland solution). Values were collected at PAR $600 \mu\text{mol}\cdot\text{m}^{-2}\cdot\text{s}^{-1}$ and 30°C . Statistical analysis was done using one-way ANOVA followed by the Fisher LSD test with a significant level < 0.05 , and errors represent SD, $n=4$.

Bibliography:

1. Evans, D.G.; Slade, R.C.T. Structural aspects of layered double hydroxides. *Struct. Bond.* **2005**, *119*, 1–87.
2. Ádok-Sipiczki, M.; Szilagyí, I.; Pálkó, I.; Pavlovic, M.; Sipos, P.; Nardin, C. Design of nucleic acid-layered double hydroxide nanohybrids. *Colloid Polym. Sci.* **2017**, *295*, 1463–1473.
3. Kuroda, Y.; Miyamoto, Y.; Hibino, M.; Yamaguchi, K.; Mizuno, N. Tripodal ligand-stabilized layered double hydroxide nanoparticles with highly exchangeable CO₃²⁻. *Chem. Mater.* **2013**, *25*, 2291–2296.